Transition between diffusion- and pressure-driven thrust of self-propelled heaving foils.

Luis Benetti Ramos[1] †, Olivier Marquet[1] and Michel Bergmann [2,3]

[1]ONERA – The French Aerospace Lab, F-92190 Meudon, France

[2]Université de Bordeaux, IMB, UMR 5251, F-33400 Talence, France

[3]Equipe-projet Memphis, Inria Bordeaux-Sud Ouest, F-33400 Talence, France

(Received xx; revised xx; accepted xx)

Flapping propulsion is a locomotion strategy adopted by living organisms whose thrust origin is normally associated to fluid acceleration rather than viscous friction. Studies show, however, that the latter diffusive forces might still play an important role on its thrust generation. In this work, we address this issue studying the diffusion and pressure time-averaged contributions to the thrust generated by a horizontally self-propelled heaving foil immersed in a quiescent fluid. Using numerical simulations we show that while increasing the flapping frequency or amplitude this system transition between two distinct thrust regimes. In the first one the time-averaged thrust is driven by viscous diffusion, with forces generated by the asymmetric shear on the foil lateral surface whereas in the second one the thrust is driven by the trailing edge pressure increase, a consequence of the fluid acceleration behind the foil. We finally study the effect of flapping amplitude and thickness-to-chord aspect ratio over these thrust regimes, highlighting that the diffusion-driven thrust regime is enhanced for smaller aspect ratios and that the transition between both regimes takes place for a constant Stokes number $\beta_A = fAc/\nu \approx 10$ based on A and f the flapping amplitude and frequency, c the foil chord and ν the fluid viscosity.

Key words:

1. Introduction

The flapping propulsion adopted by fish and birds in nature (Wu 2010; Smits 2019) is a great source of inspiration for the conception of innovative artificial swimmers (Barrett 1996; Ramananarivo *et al.* 2013). One of the key points addressed by researches and engineers that intend to interpret or reproduce this locomotion strategy is the generation of thrust forces that allow the flapping body to propel themselves through fluids. This force is generated as a response of the surrounding fluid to the flapping movement of the body, and it may greatly vary in nature according to the nature of the surrounding flow.

In this work, we are interested at the physical nature of the thrust generated by a horizontally self-propelled heaving symmetric foil in a quiescent fluid at its cruise regime. Flapping propulsion has been long conceived as a propulsive strategy based on the acceleration of the surrounding fluid (Lighthill 1971). This strategy, that generally employs a perpendicular to the travel direction motion of the flapping appendage, exploiting thus anisotropic nonlinear/convective effects of the surrounding flow to accelerate a greater mass of fluid, largely contrasts to the non-reciprocal movements of viscous swimmers that exploit isotropic viscous forces resisting against the body

† Email address for correspondence: luisbenettiramos@gmail.com

movement (Lauga 2011). However, in recent years, studies have shown that flapping propulsion is not only based on the fluid acceleration and resistive forces have been identified as key thrust components of the cruise regime of undulatory swimmers (Piñeirua *et al.* 2015), thanks to the projection by the body curvature of forces that resist against the body perpendicular motion, in the direction of swimming and at the onset of flapping propulsion Alben & Shelley (2005); Deng & Caulfield (2018), where the flow symmetry breaking around symmetrical heaving foils is followed by the emergence of simultaneous thrust contributions of viscous and pressure forces that set the foil into motion - viscous forces falling into an usual drag role only when the cruise regime is reached. To better characterize this transition between thrust and drag role of viscous forces, the present paper aims at investigating the evolution of the physical nature of the thrust of symmetric flapping wings in a quiescent fluid.

Associate the thrust production with the wake Andersen *et al.* (2017). Although some caution is needed as pointed out by Floryan *et al.* (2020) Zhang (2017) elements of the flow are still

Effect of the foil shape (Alben & Shelley 2005). Wake maps (Lu & Liao 2006; Andersen *et al.* 2017).

In this study, the physical nature of the thrust produced by a self-propelled symmetric heaving foil in a quiescent fluid is numerically investigated. We show here that there exists a transition after the onset of flapping propulsion between a diffusion and a pressure-driven thrust regime, with this study being dedicated to characterize these both regimes and the influence of the foil thickness-to-chord aspect ratio and the flapping amplitude and frequency on the transition. The description of the studied configuration and the numerical method employed are presented in §2). Simulations results are thus addressed in §3 and based on their analysis we conclude in §4 on the characteristics of the diffusion and pressure-driven thrust regimes and the existing transition between both for self-propelled heaving symmetric foils.

2. Studied configuration and numerical method

We investigate in this work the diffusion and pressure-driven thrust generated by a self-propelled heaving symmetric rectangular foil. This rectangular body (rigid with rounded edges) is characterized by its chord $c = 1$ and its non-dimensional thickness $h = h^*/c$ (where * is adopted to differentiate dimensional and nondimensional parameters) with uniform density ratio ρ_s, the diameter of the rounded edges being equal to the foil thickness. This body translates in an initially quiescent two-dimensional fluid of density ρ_f and kinematic viscosity ν with a velocity $\mathbf{u}_g = (u_g, v_g)$ that is partially imposed, with a vertical heaving motion $y_g^*(t) = -A^* \cos(2\pi f^* t^*)$, and partially free along the horizontal axis e_x as a result of hydrodynamic forces acting on the solid-fluid interface Γ_w.

This rigid-body fluid-structure interaction is characterized by four non-dimensional parameters, namely the frequency-based Stokes number β (or the flapping amplitude-based Stokes number β_A depending whether the velocity characteristic scale is based on the foil chord cf^* or the flapping amplitude $A^* f^*$), the non-dimensional amplitude A, the solid-fluid density ratio ρ and the non-dimensional thickness h, defined respectively as

$$\beta = \frac{f^* c^2}{\nu} \left(\text{or } \beta_A = \frac{A^* f^* c}{\nu} \right), \; A = \frac{A^*}{c}, \; \rho = \frac{\rho_s}{\rho_f} \text{ and } h = \frac{h^*}{c}. \tag{2.1}$$

The non-dimensional flapping period T is thus equal to 1 whatever the values of the Stokes number β, a parameter that encodes the effect of the dimensional frequency f^*. The surrounding fluid, absolute fluid velocity $\mathbf{u} = (u, v)$ and pressure p, is governed by the two-dimensional incompressible Navier-Stokes equations

$$\frac{\partial \mathbf{u}}{\partial t} = -\boldsymbol{\nabla}\mathbf{u}\cdot(\mathbf{u}-\mathbf{u}_g) - \boldsymbol{\nabla}p + \beta^{-1}\boldsymbol{\Delta}\mathbf{u}\,,\ \boldsymbol{\nabla}\cdot\mathbf{u} = 0\,, \tag{2.2}$$

written in the non-inertial frame of reference that follows the foil center of mass G as done in other fluid-structure interactions studies, such as falling and rising bodies in fluids (Jenny *et al.* 2003; Tchoufag *et al.* 2014) or pitching foils (Jallas *et al.* 2017). The body is self-propelled and the evolution of its horizontal motion is governed by Newton's second law

$$\frac{\mathrm{d}u_g}{\mathrm{d}t} = (\rho S)^{-1}F_x(\mathbf{u},p)\ ,\ F_x(\mathbf{u},p) = F_x^p(p)+F_x^\nu(\mathbf{u}) = \int_{\Gamma_w}([-p\mathbf{I}+\beta^{-1}(\boldsymbol{\nabla}\mathbf{u}+\boldsymbol{\nabla}^T\mathbf{u})]\cdot\mathbf{n})\cdot\mathbf{e}_x\mathrm{d}\Gamma_w\,, \tag{2.3}$$

where S is the non dimensional surface of the foil and $\mathbf{n}$ is the outward normal. Equations (2.2) and (2.3) are closed by a no-slip boundary condition on the foil surface $\mathbf{u}(\Gamma_w,t) = \mathbf{u}_g(t)$. In eq. (2.3) the horizontal force is decomposed in two physically distinct contributions: one that depends exclusively on the pressure F_x^p and another that depends on the diffusion F_x^ν through the velocity gradients and the Stokes number β. In this work, we will primarily evaluate the physical nature of the hydrodynamic thrust (drag) force that sustains (resist against) the motion at cruise conditions. Three important physical quantities will be studied – the time-averaged along a flapping period horizontal velocity as well as the viscous and pressure forces contributions to the total horizontal force

$$< u_g >= \int_{t_0}^{t_0+1} u_g\mathrm{d}t,\ < F_x >=< F_x^p > + < F_x^\nu >\ . \tag{2.4}$$

In the cruise regime, the time-averaged horizontal velocity is constant and the averaged horizontal force is zero, since the foil is longer accelerated. Therefore pressure and viscous components of the mean force shall mutually compensate and we can clearly identify a thrust and a resistive role, which will be employed to identify diffusion and pressure-driven thrust regimes of locomotion.

The coupled fluid-solid equations are solved numerically using the unsteady nonlinear solver described (and validated) in cite JFM, coded in the non-commercial finite-element software FreeFEM (Hecht 2012) that is second order time-accurate. The reader is referred to this reference for all technical details. In this study, we will investigate the effect of the Stokes number $1 \leqslant \beta \leqslant 300$, the flapping amplitude $0.1 \leqslant A \leqslant 0.5$ and the foil thickness $0.025 \leqslant h \leqslant 0.1$ while maintaining the density ratio $\rho = 100$ fixed. This choice of parameter is made to as to explore thicknesses, flapping frequencies and amplitudes usually employed in the literature (Alben & Shelley 2005; Lu & Liao 2006; Deng & Caulfield 2015) and a density ratio that lies in an intermediary range of the one observed for real tails and wings of swimming and flying animals ($O(10-1000)$)(Lu & Liao 2006).

3. Results and discussion

We initially consider the heaving foil for a fixed flapping amplitude $A = 0.25$, density $\rho = 100$ and aspect ratio $h = 0.05$ while varying the Stokes number $1 \leqslant \beta \leqslant 80$. As the Stokes number is increased, the temporal evolution of the foil time-averaged horizontal velocity $< u_g >$, and horizontal force total, pressure and viscous components ($< F_x >$ $< F_x^p >$ and $< F_x^\nu >$) reveals two distinct behaviours that are exemplified in figure 1 for $\beta = 14$ and $\beta = 62$. For both foils the time-averaged horizontal velocity (1-a) increases until it reaches a cruise regime where it becomes constant, with the cruise horizontal velocity being greater for the highest Stokes number. Since this velocity is positive in both cases its increase is linked to the existence of a hydrodynamic

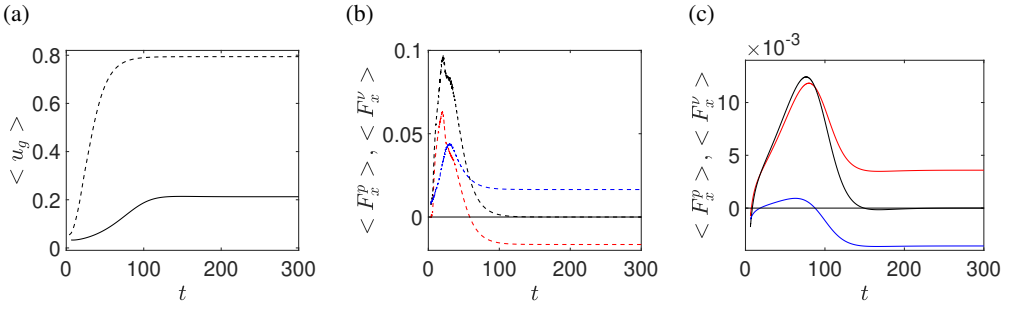

Figure 1: Temporal evolution of a diffusion-driven, Stokes number $\beta = 14$ (solid line), and a pressure-driven, $\beta = 62$ (dashed line), self-propelled solutions. (a) Horizontal velocity time-averaged over the non-dimensional flapping period $T = 1$. (b,c) Time-averaged pressure (blue) and viscous (red) components of the horizontal force (black). Parameters: $A = 0.25$, $\rho = 100$ and $h = 0.05$.

thrust, a positive horizontal force, that becomes zero in average when the cruise regime is reached, with pressure and viscous components compensating each other. In both cases, this hydrodynamic thrust is dominated by viscous forces at initial time instants but the temporal evolution at different Stokes numbers result in distinct faiths for this diffusive-driven thrust. For $\beta = 62$ (1-b), it will be surpassed by pressure contributions ($t \leqslant 50$) during the transitory regime with the viscous forces eventually turning into a classical viscous drag role ($t \geqslant 70$) that is kept during the cruise regime where the thrust is driven by pressure forces. This thrust-drag transition, observed also for other self-propelled foils (Alben & Shelley 2005; Deng & Caulfield 2018), is however not reproduced for $\beta = 14$ (1-c), where pressure contributions fall this time into a resistive role for $t \geqslant 100$ leading to a diffusive-driven thrust in the cruise regime – a behaviour never highlighted, to our knowledge, in the literature.

To understand how the foil transition between these two regimes we have studied the evolution with the Stokes number β of $< u_g >$, $< F_x^p >$ and $< F_x^\nu >$ at the foil permanent regime, as depicted in figure 2 (a) and (b). We see in (2-a) that for $\beta \geqslant 8$ $< u_g >$ starts to grow. However, its growth is not monotonous with the Stokes number and a plateau is reached for $\beta \in [23, 39]$ where $< u_g > \approx 0.35$, the velocity growth reappearing for $\beta \geqslant 40$. This non-monotonous growth of the horizontal velocity is associated to the transition between diffusion and pressure-driven thrust regimes. In figure 2 (b) we observe that for small Stokes number $8 \leqslant \beta \leqslant 39$ the thrust is dominated by diffusive forces. This thrust reaches a maximum value for $\beta = 25$, and decays after value until becoming negative for $\beta \geqslant 40$ – precisely the region of the horizontal velocity plateau. When the diffusive force finally becomes negative, it switches roles with the pressure force resulting on the transition to the pressure-driven thrust regime. The pressure forces then grow following this transition leading to the return of the velocity growth observed in (2-a).

Albeit the supposedly viscous nature of the flow for low Stokes numbers, the existence of the diffusion-driven thrust regime is surprising due to the time-reciprocal gait adopted in this case. The imposed movement is very different than the non-reciprocal gaits adopted by swimmers that rely on diffusive forces for very low Stokes numbers (Purcell 1977; Lauga 2011), which lead us to two central questions: (1) how is the diffusive-driven thrust regime originated and (2) how does it transition to a pressure-driven thrust regimes?

To answer these questions we selected three typical solutions a diffusion-driven thrust regime $\beta = 14$, a transitional $\beta = 39$ and a pressure-driven thrust regime $\beta = 62$ solution to study their flow in figure 3. We observe for the diffusion-driven thrust solution, figure 3(a-c), that no vortices are shed away from the foil. The unsteady flow depicted by the out-of-plane vorticity ω_z 3(a) consists of a pair of opposite sign vortex attached to the foil leading and trailing edge, a structure

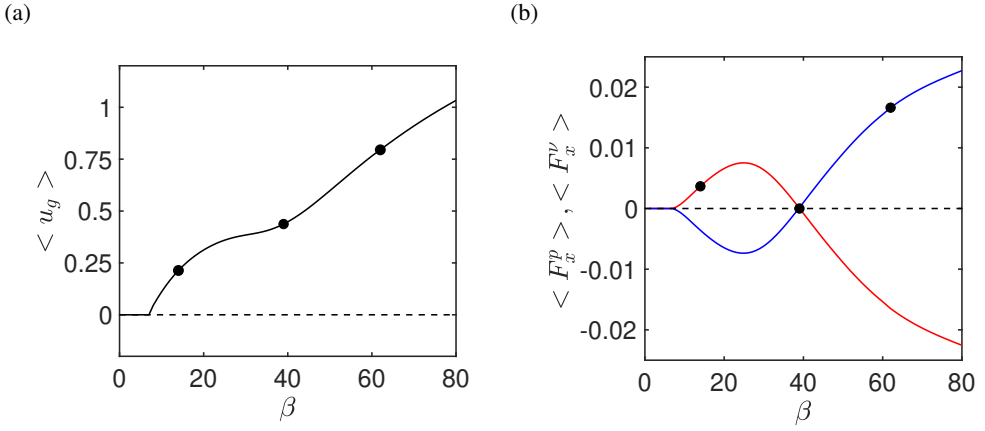

Figure 2: Time-averaged (a) horizontal velocity $< u_g >$ and (b) horizontal forces (viscous $< F_x^\nu >$ in red, pressure $< F_x^p >$ in blue) as a function of the Stokes number β. The black dashed lines indicate a zero value in both cases. Black dots indicate a diffusion-driven ($\beta = 14$), a transitional ($\beta = 39$) and a pressure-driven ($\beta = 62$) solution in presented in figure 3. Parameters: $A = 0.25$, $\rho = 100$ and $h = 0.05$.

remarkably similar to so-called *starting flows* (Lian & Huang 1989). In the present case, however, the pair of vortex breaks the left-right flow symmetry

$$(u, v, p, \omega_z)(x, y, t) = (-u, v, p, -\omega_z)(-x, y, t)\,, \tag{3.1}$$

which is at the origin of an instantaneous non-zero horizontal force (Jallas *et al.* 2017) produced by the flapping foil. This left-right asymmetry is also present in the flow time-averaged streamwise velocity (3-b), which reveals a greater spatial portion of higher value positive velocity, same orientation as the foil horizontal velocity u_g, surrounding the foil leading edge. This left-right asymmetry observed for the fluid is also present in the flow time-averaged pressure (3-c), with the minimum pressure being observed at the foil trailing edge. This flow distribution leads to the forces exhibited by the diffusion-driven thrust regime: while the velocity distribution results in an asymmetric shear profile where the leading edge positive contribution covers a greater surface of the foil than the negative contribution resulting in the diffusion-driven thrust, the trailing edge pressure minimum results in a pressure drag.

This shear asymmetry and pressure drag is progressively erased by the increase of the Stokes number. At the transitional solution, figure 3(d-f), we can see that the flow is no longer similar to a starting flow, with the trailing edge featuring now a vortex dipole (3-d). This dipole has been observed in the transition to horizontal motion (Alben & Shelley 2005) and associated to a reduction of the trailing edge suction force. This reduction comes from the increase of negative velocity at the foil trailing edge (3-e), indicating an increase of the fluid acceleration to the left opposite to the foil travel direction (right). The positive velocity around the foil leading edge is reduced when compared to the diffusive-thrust solution. The pressure (3-f) becomes more left-right asymmetric with a decrease of its value behind the trailing edge. The decrease of the trailing edge suction and of the leading edge shear result in the decay of the diffusion-driven thrust and the pressure drag. When this transition point is passed, the vortex will no longer remain attached to the trailing edge and a reversed Von-Kármán wake (Triantafyllou *et al.* 1991) is formed by the vortex shed by the wing a characteristic of the pressure-driven thrust solution, depicted in figure 3(g-i). The time-averaged flow (3-h) consists thus of a jet of negative horizontal velocity behind the foil trailing edge, and the fluid acceleration behind the foil is thus enhanced and a large zone

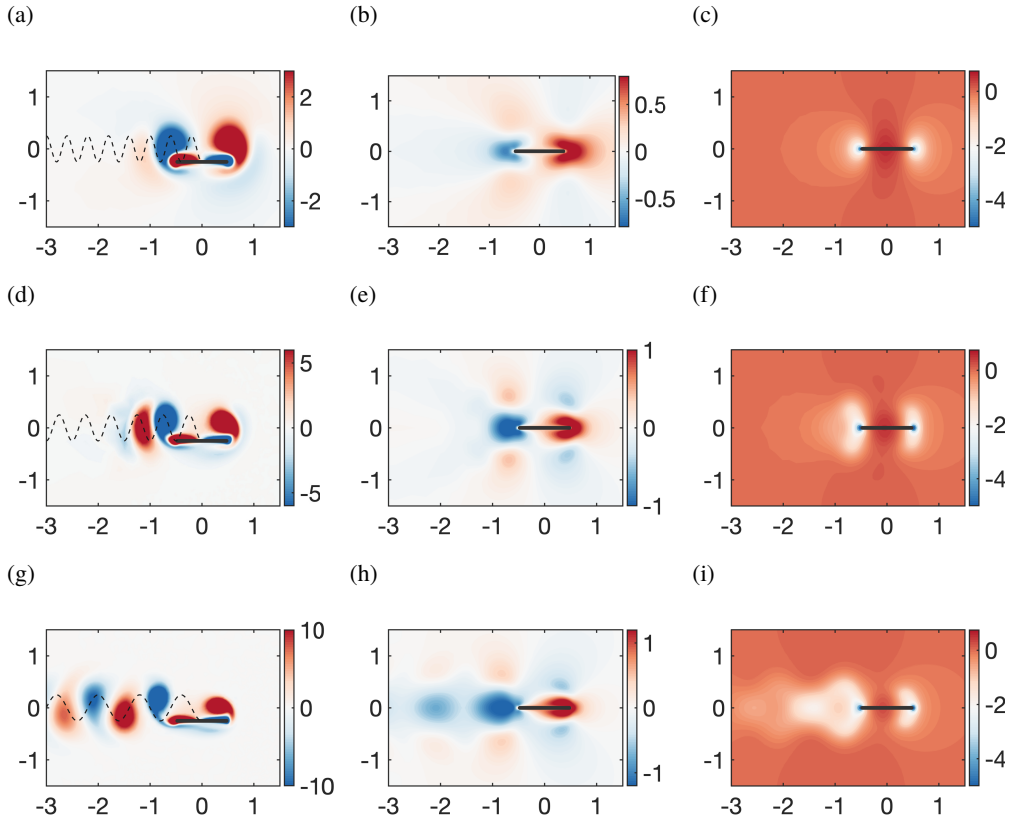

Figure 3: (a-c) Diffusion-driven ($\beta = 14$) (d-f) transitional ($\beta = 39$) and (g-i) pressure-driven ($\beta = 62$) self-propelled solutions. (a,d,g) Instantaneous vorticity field, (b,e,h) Time-averaged stream-wise velocity u field and (c,f,i) the time-averaged pressure p field. The dashed lines in (a,d,g) correspond to the foil center of mass trajectory.

of pressure decrease is visible behind the foil trailing edge (3-i). The pressure balance is thus shifted, with the trailing edge suction being significantly reduced when compared to the leading edge forces, which finally results in a pressure-driven thrust force.

Since diffusion and pressure driven thrust solutions present very different flow spatial distributions around the surface of this rectangular foil with rounded edges foil, we decompose the viscous forces ($< F_x^\nu >=< F_L^\nu > + < F_E^\nu >$) in components integrated over the flat lateral walls $< F_L^\nu >$ and round leading/trailing edges $< F_E^\nu >$ and the pressure forces ($< F_x^p >=< F_+^p > - < F_-^p >$) over the leading $< F_+^p >$ and $< F_-^p >$ trailing edge. The evolution of these contributions with the Stokes numbers, figure 4, reveals that the diffusion driven thrust is generated by diffusive forces alongside the foil lateral wall $< F_L^\nu >$ (4-a), with this component being thrust producer (positive) for all the investigated β and growing for $\beta \leqslant 25$, while diffusive forces on the foil edge $< F_E^\nu >$ are always negative. The diffusion-driven thrust appears thus to be generated by the previously identified shear asymmetry alongside the lateral wall and the predominant positive streamwise velocity alongside the foil surface (as seen in 3-b). It is interesting to note that forces associated to starting flows were highlighted by Piñeirua *et al.* (2015) as the thrust source of low aspect ratio anguilliform swimmers. In their case, however, the thrust is originated by a projection of

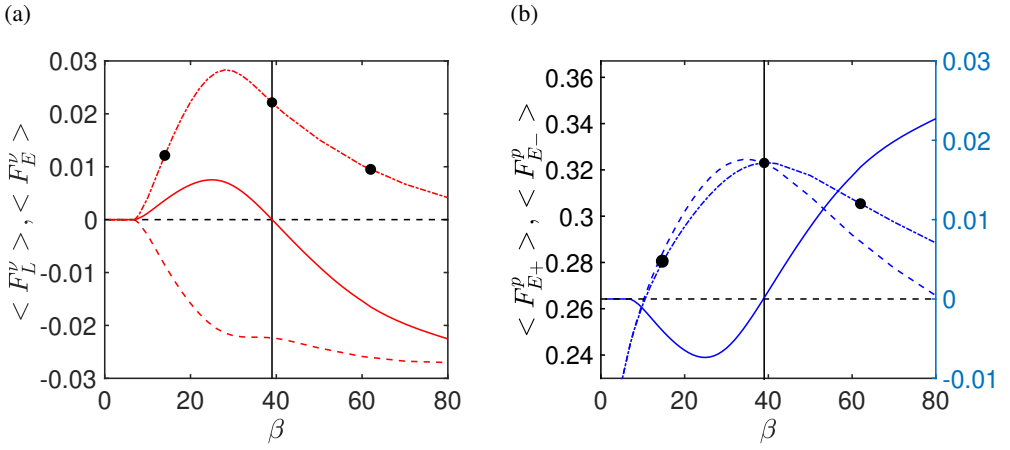

Figure 4: Evolution with the Stokes number β of (a) viscous forces lateral-wall $< F_L^\nu >$ (dash-dotted) and leading/trailing edges $< F_E^\nu >$ (dashed) contributions and (b) pressure forces leading-edge $< F_{E+}^p >$ (dash-dotted) and trailing-edge $< F_{E-}^p >$ (dashed) contributions. In all figures solid lines represent the total force and the vertical line delimits the transition between diffusion and pressure-driven regimes. In (b) the total force values are fixed on the right axis.

this perpendicular force through the body curvature on the swimming direction, different than our case, where the "projection" is generated by the flow left-right asymmetry.

The transition from diffusive to pressure-driven thrust is dictated by the decay of the diffusive forces and of the pressure trailing edge $< F_-^p >$ suction force generated by the apparition of the vortex dipole and the time-averaged jet behind the foil for $\beta \geqslant 39$. Similar to the predictions of Lighthill (1969), the propulsion in the pressure-driven regime is driven by the fluid acceleration in the foil trailing edge. The late transition to a regime where the fluid acceleration around the trailing edge grants a thrust enhancement might have important implications for systems with passive elasticity that allows a greater trailing edge flapping amplitude than the leading edge Spagnolie *et al.* (2010). We remark that the transition between diffusion and pressure-driven thrust regimes might be in the origin of the small influence observed in the literature of the passive elasticity for low β since the diffusive-driven thrust regime does not rely on the trailing edge fluid acceleration.

As the diffusion-driven thrust is mainly generated by the foil lateral wall, we have studied its sensibility to the thickness-to-chord aspect ratio in the range $0.025 \leqslant h \leqslant 0.1$. As seen in figure 5, an increase of the aspect ratio, that reduces the foil lateral surface, has a great impact on the evolution of the time-averaged horizontal velocity and viscous horizontal force. First of all, the foil time-averaged horizontal velocity $< u_g >$ and viscous force $< F_x^\nu >$ are enhanced for the smaller aspect ratios. For the smallest thickness ($h = 0.025$) the horizontal velocity permanently grows, and as h is increased, the evolution with β of the velocity becomes less monotonous. At $h = 0.075$ the evolution becomes non-continuous and quasi-periodic propulsive solutions, identified by a dashed grey line, emerge. These solutions, already investigated in the literature (Alben & Shelley 2005; Lu & Liao 2006), and non-coherent states where the foil exhibits a back & forth motion around a fixed point in space. We suppose that these solutions emerge due to the decrease of foil velocity that becomes incapable of attaining the transition between the thrust and drag role of viscosity that is exhibited in figure 1. While the aspect ratio present a small influence on the locomotion onset, attained for $\beta \sim 10$, the transition between thrust regimes is greatly impacted. It first decreases between $h = 0.025$ and $h = 0.05$ from $\beta = 46$ to $\beta = 39$.

(a) (b)

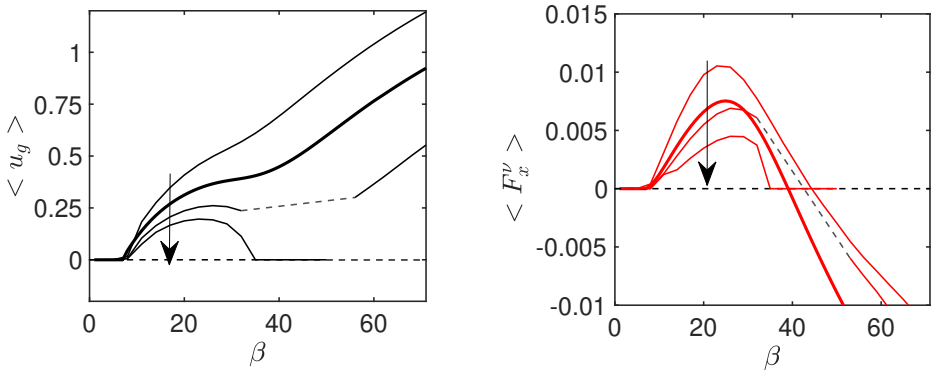

Figure 5: Evolution with the Stokes number for four different non-dimensional thickness $h = 0.025$, $h = 0.05$ (previous treated case and thicker line), $h = 0.075$ and $h = 0.1$ (arrow indicating the direction of aspect ratio growth in both figures) of the time-averaged horizontal (a) velocity $< u_g >$ and (b) viscous force component $< F_x^v >$. The solid lines correspond to periodic solutions, whereas grey dotted lines to quasi-periodic solutions, the latter being found for $h = 0.075$ and $h = 0.1$. In both figures, a black dotted line indicate zero values.

Although non-coherent states of locomotion emerge, we can predict that the β threshold for this transition is greater beyond $h = 0.075$, due to the non-continuous evolution of the viscous force in (1-b) as well as the fact that for $h = 0.1$ the transition to pressure-driven thrust is not observed for $\beta \leqslant 80$. For this aspect ratio the diffusion-driven thrust regime is suppressed for $\beta = 33$ and symmetric non-propulsive solutions are obtained beyond this value, with non-coherent solutions being obtained for $\beta \geqslant 52$.

In order to further characterize the transition between diffusion and pressure-driven thrust regimes, the influence of the flapping amplitude on the foil thrust regimes is investigated in the plan (A, β) and (A, β_A). Figure 6 depicts the value of the time-averaged diffusive component of the horizontal force in these plans. Since diffusion and pressure forces mutually compensate in cruising regimes, regions where $< F_x^v >$ is positive (negative) correspond to a diffusion-driven (pressure-driven) regime. It can be seen in this figure that the first transition obtained for all flapping amplitudes while increasing the Stokes numbers β or β_A is the transition between a non-propulsive (white background) and diffusion-driven thrust (red background) regime that takes place for an almost constant $\beta_A \approx 3$ (similar to the case of an ellipse of non-dimensional thickness $h = 0.1$ (Deng & Caulfield 2015)). This predominance indicates the importance of this thrust regime for the flapping propulsion onset and can be correlated to the one observed at the onset of locomotion in transient regimes (figure 3). The transition between diffusion and pressure-driven thrust is thus obtained with the increase of the Stokes number, again for an almost constant $\beta_A \approx 10$, particularly true for small amplitudes $A \leqslant 0.3$ with this frontier growing up to $\beta_A = 13.5$ for $A = 0.5$. The delay of the transition to pressure-driven thrust regimes for higher flapping amplitudes is connected to the emergence of non-coherent states of locomotion that interrupt the continuous evolution of the foil velocity (as seen in figure 5) which postpones the emergence of vortex wakes and the transition to pressure-driven regimes. Comparing the results in the plans (A, β) and (A, β_A) we remark that both the transition between non-propulsive and diffusion-driven thrust regimes and the two thrust regimes are better characterized by the flapping

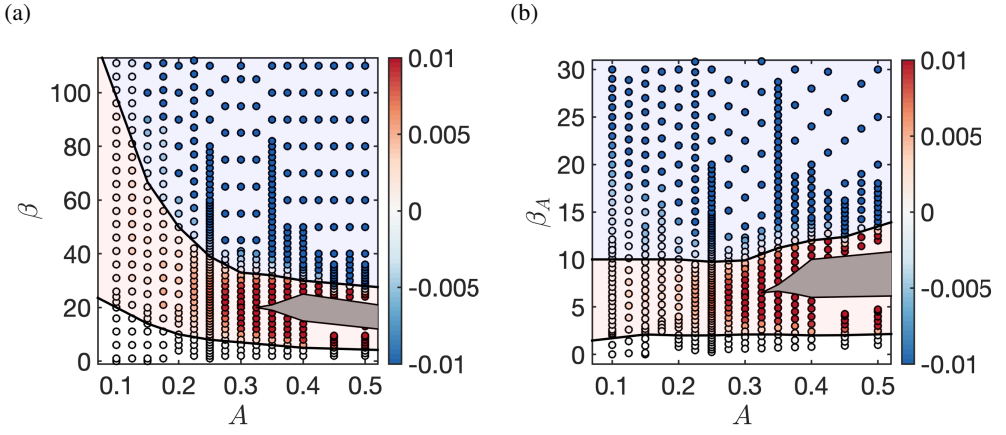

Figure 6: Diffusion-driven and pressure-driven self-propelled regimes in the parameter space (a) (A, β) and (b) (A, β_A) where $\beta_A = A\,\beta$. Filled circles represent the value of the time-averaged viscous force. Since $< F_x^v >= - < F_x^p >$ positive and negative regions correspond to diffusion or pressure-driven thrust regimes, further identified by red and blue background colors. White regions correspond to non-propulsive solutions. The black curves delimit the transition between those regimes. Grey regions correspond to non-coherent quasi-periodic solutions. Fixed control parameters are $h = 0.05$ and $\rho = 100$.

amplitude based Stokes number β_A. This indicate that the transitions are somehow linked to a sufficient foil vertical velocity that generates the flow symmetry breaking and the emergence of a vortex wake, thus granting the onset of diffusion and pressure-driven thrust regimes.

4. Conclusions

In this work, we have investigated the time-averaged contributions of diffusion and pressure forces to the horizontal forces generated by a horizontally self-propelled heaving foil in a quiescent fluid. We have highlighted the existence of a transition between diffusion and pressure-driven thrust regimes. By studying the time-averaged flow associated to each of these regimes, we have shown that the diffusion-driven thrust is based on the asymmetric shear on the foil lateral surface, whereas the pressure-driven thrust regime relies on the fluid acceleration behind the flapping body and its consequent reduction of the trailing edge suction force. We have finally studied the influence of the thickness-to-chord aspect ratio and the flapping amplitude, revealing that the diffusive-driven thrust is enhanced for smaller thickness-to-chord aspect ratios and might be mitigated for greater ones. In the flapping amplitude and frequency plan, the transition between these thrust regimes takes place for a flapping amplitude based Stokes number $\beta_A \approx 10$ with this frontier increasing in value for higher amplitudes of motion where non-coherent states of locomotion emerge.

Declaration of Interests: The authors report no conflict of interest.

Acknowledgments

This project has received funding from the European Research Council (ERC) under the European Union Horizon 2020 research and innovation program (grant agreement No.638307)

REFERENCES

Alben, Silas & Shelley, Michael 2005 Coherent locomotion as an attracting state for a free flapping

body. *Proceedings of the National Academy of Sciences of the United States of America* **102** (32), 11163–11166.

Andersen, A., Bohr, T., Schnipper, T. & Walther, J. H. 2017 Wake structure and thrust generation of a flapping foil in two-dimensional flow. *Journal of Fluid Mechanics* **812**, R4.

Barrett, David Scott 1996 *Propulsive Efficiency of a Flexible Hull Underwater Vehicle*.

Deng, Jian & Caulfield, C. P. 2015 Dependence on aspect ratio of symmetry breaking for oscillating foils: Implications for flapping flight. *Journal of Fluid Mechanics* **787**, 16–49.

Deng, Jian & Caulfield, C. P. 2018 Horizontal locomotion of a vertically flapping oblate spheroid. *Journal of Fluid Mechanics* **840**, 688–708.

Floryan, Daniel, Buren, Tyler Van & Smits, Alexander J 2020 Swimmers' wake structures are not reliable indicators of swimming performance. *Bioinspiration & Biomimetics* **15** (2), 024001.

Hecht, Frédéric 2012 New development in freefem ++ Frédéric Hecht To cite this version : HAL Id : hal-01476313. *Journal of Numerical Mathematics* **20** (3), 1–14.

Jallas, Damien, Marquet, Olivier & Fabre, David 2017 Linear and nonlinear perturbation analysis of the symmetry breaking in time-periodic propulsive wakes. *Physical Review E* **95** (6), 1–15.

Jenny, Mathieu, Bouchet, Gilles & Dušek, Jan 2003 Nonvertical ascension or fall of a free sphere in a Newtonian fluid. *Physics of Fluids* **15** (1), L9–L12.

Lauga, Eric 2011 Life around the scallop theorem. *Soft Matter* **7** (7), 3060–3065, arXiv: 1011.3051.

Lian, Q. X. & Huang, Z. 1989 Starting flow and structures of the starting vortex behind bluff bodies with sharp edges. *Experiments in Fluids* **8** (1-2), 95–103.

Lighthill, M J 1969 Hydromechanics of aquatic animal propulsion. *Annual Review of Fluid Mechanics* **1** (1), 413–446.

Lighthill, M. J. 1971 Large-Amplitude Elongated-Body Theory of Fish Locomotion. *Proceedings of the Royal Society B: Biological Sciences* **179** (1055), 125–138.

Lu, Xi Y. & Liao, Qin 2006 Dynamic responses of a two-dimensional flapping foil motion. *Physics of Fluids* **18** (9).

Piñeirua, M., Godoy-Diana, R. & Thiria, B. 2015 Resistive thrust production can be as crucial as added mass mechanisms for inertial undulatory swimmers. *Physical Review E - Statistical, Nonlinear, and Soft Matter Physics* **92** (2), 1–6, arXiv: 1507.04952.

Purcell, E. M. 1977 Life at low Reynolds number. *American Journal of Physics* **45** (1), 3–11, arXiv: arXiv:1011.1669v3.

Ramananarivo, Sophie, Godoy-Diana, Ramiro & Thiria, Benjamin 2013 Passive elastic mechanism to mimic fish-muscle action in anguilliform swimming. *Journal of the Royal Society Interface* **10** (88).

Smits, Alexander J 2019 Undulatory and oscillatory swimming. *Journal of Fluid Mechanics* **874**.

Spagnolie, Saverio E., Moret, Lionel, Shelley, Michael J. & Zhang, Jun 2010 Surprising behaviors in flapping locomotion with passive pitching. *Physics of Fluids* **22** (4), 1–20.

Tchoufag, Joël, Fabre, David & Magnaudet, Jacques 2014 Global linear stability analysis of the wake and path of buoyancy-driven disks and thin cylinders. *Journal of Fluid Mechanics* .

Triantafyllou, M. S., Triantafyllou, G. S. & Gopalkrishnan, R. 1991 Wake mechanics for thrust generation in oscillating foils. *Physics of Fluids A* **3** (12), 2835–2837.

Wu, Theodore Yaotsu 2010 A Review on Fish Swimming and Bird/Insect Flight. *Annual Review of Fluid Mechanics* **43** (1), 25–58, arXiv: 1006.1927.

Zhang, Jun 2017 Footprints of a flapping wing. *Journal of Fluid Mechanics* **818**, 1–4.